PERGAMON

International Journal of Heat and Mass Transfer 44 (2001) 1235–1247

International Journal of HEAT and MASS TRANSFER

www.elsevier.com/locate/ijhmt

Numerical simulation of steady and transient mass transfer to a single drop dominated by external resistance

Zai-Sha Mao *, Tianwen Li [1], Jiayong Chen

Institute of Chemical Metallurgy, Chinese Academy of Sciences, Beijing 100080, China

Received 5 February 2000; received in revised form 22 April 2000

Abstract

In a boundary-fitted orthogonal coordinate system, the general governing equations for steady and transient axisymmetrical cases of mass transfer in the external region around single buoyancy-driven drops in steady motion under low or intermediate Reynolds number were expanded and numerically solved by the control volume formulation. The simulation results for typical cases were presented and compared well with the data and empirical correlations in the literature. It suggests that the developed mathematical formulation of the external mass transfer for a deformable buoyancy-driven drop is reasonable, and may give reliable simulating results. The analysis of the mass transfer coefficient against the detail of flow near the drop interface shed light to the respective contribution of molecular diffusion, convection and recirculating wake, as to provide information on the characteristic time scale of decaying Sherwood number, and hence, to be valuable for analyzing and optimizing the solvent extraction operation.

Keywords: Mass transfer; Single drop; Numerical simulation; Extraction

1. Introduction

Liquid–liquid extraction is widely used for mass transfer unit operation, in which the solute is transferred mainly between liquid drops (single drop or drop swarm) and the second immiscible continuous phase. This makes mass transfer to (or from) a single drop an essential base for better understanding of liquid extraction process and for scientific design of the equipment. The mass transfer occurs in successive stages: drop formation, motion through the continuous phase, and coalescence of drops at the terminal interface. The single drop mass transfer has been quantified by means of many experimental approaches, but theoretical investigation remains rather difficult due to the transient nature of drop formation and associated mass transfer as well as the influence of many relevant factors as pointed by Clift et al. [1]. The steady buoyancy-driven motion of a single drop in an infinite immiscible liquid medium is the easiest target to be tacked theoretically. Considering the complexity of extraction process and the difficulties involved in experimental measurement, many researchers have tried to develop general models and correlations based on experimental data and simplified analytical solution so as to predict the rate of mass transfer during drop movement. Unfortunately, it seems no satisfactory model has been developed successfully which may be applied in a reasonably wide range of the drop Reynolds number. In view of the situation, numerical simulation of mass transfer to liquid drops by computational fluid mechanics (CFD) has gained progressive popularity in recent years (e.g. [2,3]).

The process of mass transfer is simulated numerically starting from hydrodynamics of a single drop moving steadily in an infinite immiscible fluid medium. Ryskin and Leal simulated the steady buoyancy-driven motion of a deformable bubble with intermediate Reynolds

* Corresponding author.

[1] Present address: Technical Center, LTH Natural Gas Chemical (Group) Co., Luzhou 646300, China.

0017-9310/01/$ - see front matter
PII: S0017-9310(00)00140-X

Nomenclature

c	concentration in continuous phase (mol/m^3)
C	dimensionless concentration in continuous phase
D	cell diffusive flux, dimensionless
D	molecular diffusivity of solute (m^2/s)
f	distortion function
e	general unit vector along a coordinate axis
F	cell convective flux, dimensionless
h_ξ, h_η	scaling factor (m)
H_ξ, H_η	dimensionless scaling factor
k	mass transfer coefficient (m/s)
N	molar flux (mol/m^2 s)
P	cell Peclet number in Eq. (30) (dimensionless)
Pe	Peclet number for mass transfer, $2RU/\mathbf{D}$
R	volume-equivalent drop radius (m)
Re	Reynolds number, $2RU\rho/\mu$ (dimensionless)
Sc	Schmidt number, $\mu/\rho\mathbf{D}$ (dimensionless)
Sh	Sherwood number, $2Rk/\mathbf{D}$ (dimensionless)
t	time (s)
u	velocity component (m/s)
U	terminal velocity (m/s)
We	Weber number, $2RU^2\rho/\sigma$ (dimensionless)
x, y	coordinate in physical plane
X, Y	dimensionless coordinate

Greek symbols

α_a	fraction of surface active in mass transfer in Table 1
β	adjusting factor
ζ	relative density ρ_2/ρ_1
θ	dimesionless time, tU/R
λ	relative viscosity μ_2/μ_1
μ	viscosity (Pa s)
ξ, η	coordinate in computational plane, $0 \leqslant \xi, \eta \leqslant 1$
ρ	density (kg/m^3)
$\tau_{0.9}$	characteristic decay time (*Sh* dropped by 90%)
ψ	stream function (dimensionless)
ω	vorticity (dimensionless)

Subscripts

1	drop
2	continuous phase
n, s, e, w	cell face label
N, S, E, W, P	node label

Superscripts

0	previous time step
∞	remote boundary
S	drop surface

numbers by the stream function–vorticity formulation in an orthogonal boundary-fitted coordinate system [4]. Ryskin and Leal [5] proposed an efficient technique for numerical generation of body-fitted orthogonal grids in both internal and external domains of a liquid drop. The technique was later extended to the case of a liquid drop with considerable deformation by Dandy and Leal [6]. The above-mentioned studies were carried out by finite difference method (FDM). The present authors were encountered with technical difficulty of accurate enforcement of the remote boundary conditions, they found that suitable designation of the distortion function would be very important. A reasonable sample of such a distortion function was presented and a plausible explanation of better numerical accuracy was suggested [7,8]. Miksis et al. [9], Haywood et al. [10,11] also studied the motion of a bubble or drop in an infinite fluid medium by FDM. Wham et al. [12] examined the wall effect on the flow structure and drag coefficient related to single drops under intermediate Reynolds number in a tube using FEM. Tomiyama et al. [13] investigated the steady motion of single bubbles under laminar conditions using the volume of fluid (VOF) method. Recently, the level set method was more often resorted to capture the topological behavior of bubbles and drops [14]. Lu and Chang [15] used the boundary element method to study the motion of a large bubble in a vertical tube. Moreover, the adaptive mesh can be adopted to improve the interface tracking technique [16].

Mass transfer between a moving single drop and the continuous phase is a topic of common interest for different technical applications. Haywood et al. [10,11] simulated transient evaporation of fuel drops and heat transfer under the typical conditions of spraying evaporation using the finite-volume formulation on a non-orthogonal grid. Comer and Kleinstreuer [17] investigated numerically the heat transfer from oblate spheroidal fuel drop with fixed aspect ratio in a tube by the FEM. In a conference paper, Li et al. [7] presented a preliminary report on the simulation of external mass transfer from the continuous phase to single drops in two extraction systems dominated by mass transfer resistance in the drop exterior.

In this paper, detail on the simulation of steady-state mass transfer dominated by the external resistance for significantly deformed single drops are presented. The numerical results were compared with the earlier data of Su et al. [18]. Numerical experiments were conducted on the effect of physical properties of the extraction system, and the mechanism underlying the influence is explored by analyzing the detailed local mass transfer along the interface. The transient behavior of external mass transfer has been investigated for typical cases relevant to practical solvent extraction systems.

2. Boundary-fitted coordinate transformation and fluid flow

The steady buoyancy-driven motion of a falling drop is time dependent, but it becomes steady state as the reference frame is attached onto the falling drop as depicted in Fig. 1. In this case, the liquid motion inside and around the drop will be governed by the non-dimensional Navier–Stokes equation

$$\mathbf{u}\cdot\nabla\mathbf{u} = -\frac{1}{2}\nabla p + \frac{2}{Re}\nabla^2\mathbf{u}, \tag{1}$$

where $\mathbf{u}$ is the non-dimensional velocity vector and p the dynamic pressure. It should be noted that Eq. (1) is non-dimensionalized with the drop radius, the physical properties of the continuous phase and the drop terminal velocity. When the steady flow field related to the drop is solved, the information contained in the flow field is further used to solve the steady or unsteady mass transfer from the continuous phase to the drop.

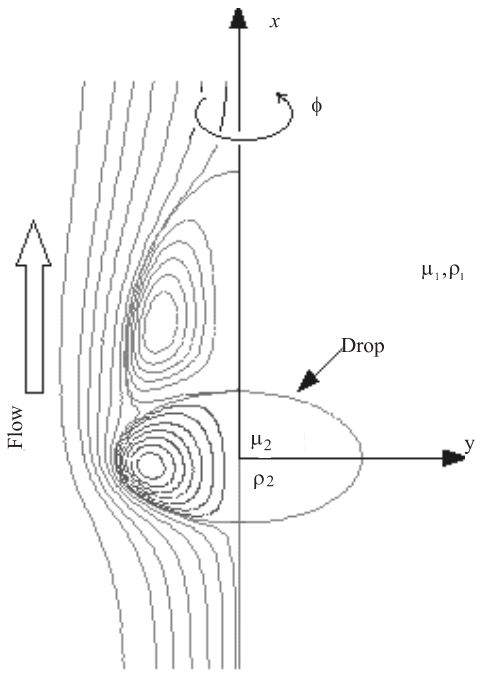

Fig. 1. Sketch of a single liquid drop moving in the fluid medium with the reference frame attached to the falling drop.

2.1. Boundary-fitted coordinate system

The buoyancy-driven motion of a single drop (disperse phase) in an infinite quiescent immiscible liquid phase (continuous phase) may subject to significant deformation, and therefore, its simulation is associated with geometric complexity of the solution domain. An orthogonal curvilinear coordinate system is beneficial to the numerical solution of drop motion and subsequent mass transfer. The covariant Laplacian Eq. (2) are utilized to transform the physical domains inside and outside a liquid drop into a unit square in the computational plane (ξ,η) as indicated in Fig. 2. Orthogonal mapping was carried out by the methods proposed by Ryskin and Leal [5]. The partial differential equations for orthogonal transform would be

$$\begin{aligned}\frac{\partial}{\partial\xi}\left(f\frac{\partial x}{\partial\xi}\right)+\frac{\partial}{\partial\eta}\left(\frac{1}{f}\frac{\partial x}{\partial\eta}\right)=0,\\ \frac{\partial}{\partial\xi}\left(f\frac{\partial y}{\partial\xi}\right)+\frac{\partial}{\partial\eta}\left(\frac{1}{f}\frac{\partial y}{\partial\eta}\right)=0\end{aligned} \tag{2}$$

and the distortion function for a finite external domain is given as [19]

$$f(\xi,\eta)=\frac{\pi}{\beta}(1-0.5\cos\pi\eta), \tag{3}$$

which defines the ratio of scaling factors in the ξ and η directions and symbolizes the aspect ratio of a cell in the physical (x, y) plane:

$$f(\xi,\eta)=\frac{h_\eta}{h_\xi}, \tag{4}$$

$$\begin{aligned}h_\xi&=\sqrt{\left(\frac{\partial x}{\partial\xi}\right)^2+\left(\frac{\partial y}{\partial\xi}\right)^2},\\ h_\eta&=\sqrt{\left(\frac{\partial x}{\partial\eta}\right)^2+\left(\frac{\partial y}{\partial\eta}\right)^2}.\end{aligned} \tag{5}$$

The scaling factors h_ξ, h_η are also called the Lamé coefficients, and β is an adjusting factor to decide the size of external domain. With proper boundary conditions relating the physical domains and the computational domain, the numerical grids are generated by solving Eq. (2) by FDM. When a drop is gradually converged to its equilibrium shape in the course of simulation, the grids must be refreshed iteratively to be adapted to the

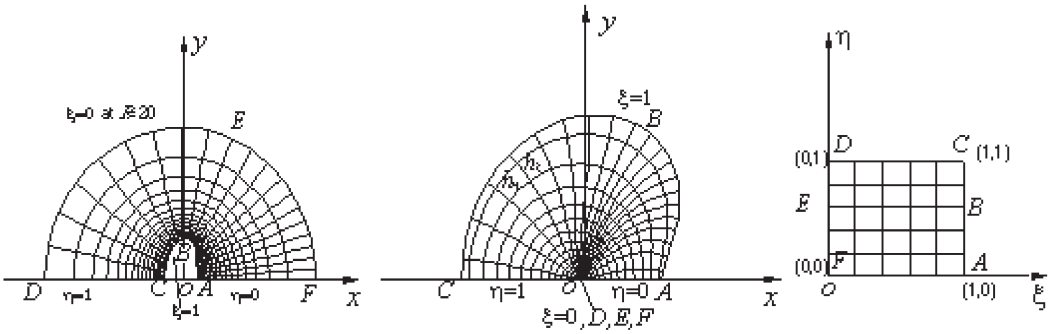

Fig. 2. The correspondence of exterior and interior of a deformable drop with the computational domain: (a) external domain; (b) drop interior; (c) unit square in (ξ,η).

shape change. The details can be referred to Ryskin and Leal [5] and Li [3].

2.2. Simulation of fluid flow

A drop moving steadily at the terminal velocity U in an infinite immiscible liquid medium may be formulated in the coordinate system fixed on the drop with the following assumptions:

1. Two fluids are viscous, incompressible and Newtonian.
2. Flow in both phases is laminar, steady state and axisymmetric.
3. The system is not contaminated by surfactant and the surface tension at the liquid–liquid interface remains constant.

The dimensionless form of Navier–Stokes equations for axisymmetric fluid flow of a buoyancy-driven single drop in terms of stream function and vorticity (with subscript 1 denoting the external domain and 2 for the drop interior) could be written as

$$L_1^2(Y_1\omega_1) - \frac{Re_1}{2}\frac{1}{H_{\xi_1}H_{\eta_1}} \times \left[\frac{\partial\psi_1}{\partial\xi_1}\frac{\partial}{\partial\eta_1}\left(\frac{\omega_1}{Y_1}\right) - \frac{\partial\psi_1}{\partial\eta_1}\frac{\partial}{\partial\xi_1}\left(\frac{\omega_1}{Y_1}\right)\right] = 0, \tag{6}$$

$$L_1^2\psi_1 + \omega_1 = 0, \tag{7}$$

$$L_2^2(Y_2\omega_2) + \frac{Re_2}{2}\frac{1}{H_{\xi_2}H_{\eta_2}} \times \left[\frac{\partial\psi_2}{\partial\xi_2}\frac{\partial}{\partial\eta_2}\left(\frac{\omega_2}{Y_2}\right) - \frac{\partial\psi_2}{\partial\eta_2}\frac{\partial}{\partial\xi_2}\left(\frac{\omega_2}{Y_2}\right)\right] = 0, \tag{8}$$

$$L_2^2\psi_2 + \omega_2 = 0, \tag{9}$$

$$L^2 = \frac{1}{H_\xi H_\eta}\left[\frac{\partial}{\partial\xi}\left(\frac{f}{Y}\frac{\partial}{\partial\xi}\right) + \frac{\partial}{\partial\eta}\left(\frac{1}{fY}\frac{\partial}{\partial\eta}\right)\right]. \tag{10}$$

Numerical solution of Eqs. (6)–(9) under suitable boundary conditions gives the external and internal flow fields and the flow parameters relevant for subsequent numerical simulation of interphase mass transfer. The details of numerical solution of fluid flow can be referred to that reported by Dandy and Leal [6] and Li et al. [8].

3. Numerical simulation of mass transfer to/from a liquid drop

3.1. Formulation

The typical situation of mass transfer to a drop is that a deformable drop rises or falls steadily at the terminal velocity U in an immiscible liquid medium is referred to Fig. 1, and for a liquid drop under low/intermediate Reynolds number, the following additional assumptions would be reasonable and generally justified:

1. The physical properties of fluids and flow structure are not influenced by the concentration of solute to be extracted, thus the solution of convective diffusion equation for both phases is uncoupled from the solution of liquid flow.
2. Thermodynamic equilibrium exists for the solute between phases at the interface, i.e. no interfacial resistance to mass transfer. When mass transfer resistance is dominated by the continuous phase, the interfacial concentration will be approximately equal to zero for very large value of the distribution coefficient of solute between drop and the continuous phase.

For the case with constant physical properties of both liquid phases, including that on the interface, the solution for mass transfer would be decoupled from the problem of fluid flow. Thus the information of the flow field, required for solution of convective diffusion problem, can be provided directly from the numerical simulation of steady-state fluid flow. In this aspect, the computer simulation of the buoyancy-driven single

drops was conducted previously [8] as the basis for numerical simulation of mass transfer to/from the liquid drop.

In general, the transient mass transfer to/from the drop is governed by the convective diffusion equation in the vector form:

$$\frac{\partial c}{\partial t}+\mathbf{u}\cdot\nabla c=\mathbf{D}\nabla^2 c. \tag{11}$$

The expanded form of the Laplacian operator in a general curvilinear coordinate system will be

$$\nabla^2=\frac{1}{h_1h_2h_3}\left[\frac{\partial}{\partial x_1}\left(\frac{h_2h_3}{h_1}\frac{\partial}{\partial x_1}\right)+\frac{\partial}{\partial x_2}\left(\frac{h_3h_1}{h_2}\frac{\partial}{\partial x_2}\right)+\frac{\partial}{\partial x_3}\left(\frac{h_1h_2}{h_3}\frac{\partial}{\partial x_3}\right)\right]$$

and the Hamilton operator is

$$\nabla=\mathbf{e}_1\frac{1}{h_1}\frac{\partial}{\partial x_1}+\mathbf{e}_2\frac{1}{h_2}\frac{\partial}{\partial x_2}+\mathbf{e}_3\frac{1}{h_3}\frac{\partial}{\partial x_3},$$

where $h_1,\ h_2,\ h_3$ are the Lamé coefficients in the x_1,x_2,x_3 directions of the generalized curvilinear coordinate system. Hence, Eq. (11) reads

$$\frac{\partial c}{\partial t}+u_1\frac{1}{h_1}\frac{\partial c}{\partial x_1}+u_2\frac{1}{h_2}\frac{\partial c}{\partial x_2}+u_3\frac{1}{h_3}\frac{\partial c}{\partial x_3}=\frac{\mathbf{D}}{h_1h_2h_3}\left[\frac{\partial}{\partial x_1}\left(\frac{h_2h_3}{h_1}\frac{\partial c}{\partial x_1}\right)+\frac{\partial}{\partial x_2}\left(\frac{h_3h_1}{h_2}\frac{\partial c}{\partial x_2}\right)+\frac{\partial}{\partial x_3}\left(\frac{h_1h_2}{h_3}\frac{\partial c}{\partial x_3}\right)\right]. \tag{12}$$

For two-dimensional axisymmetric flow with x_3 being the azimuthal angle around the axis of symmetry ϕ as indicated in Fig. 1, let x_1 and x_2 being coordinates ξ and η, respectively, in a boundary-fitted orthogonal reference frame, the correspondence between the Lamé coefficients is as follows:

$$h_1\to h_\xi,\quad x_1\to\xi$$

$$h_2\to h_\eta,\quad x_2\to\eta$$

$$h_3\to h_\phi=y,\quad x_3\to\phi.$$

The detail on selecting a coordinate system is referred to Ryskin and Leal [4,5] and Li et al. [8], notice that $h_3=y$, which is the local distance to the axis of symmetry, Eq. (12) can be reduced to the form

$$\frac{\partial c}{\partial t}+\frac{u_\xi}{h_\xi}\frac{\partial c}{\partial\xi}+\frac{u_\eta}{h_\eta}\frac{\partial c}{\partial\eta}=\frac{\mathbf{D}}{h_\xi h_\eta y}\left[\frac{\partial}{\partial\xi}\left(\frac{h_\eta y}{h_\xi}\frac{\partial c}{\partial\xi}\right)+\frac{\partial}{\partial\eta}\left(\frac{h_\xi y}{h_\eta}\frac{\partial c}{\partial\eta}\right)\right]. \tag{13}$$

Using c^∞, R and U as the non-dimensionalizing factors, Eq. (13) could be non-dimensionalized to

$$\left(\frac{Pe}{2}H_\xi H_\eta Y\right)\frac{\partial C}{\partial\theta}+\frac{Pe}{2}\left[\frac{\partial}{\partial\xi}\left(-\frac{\partial\psi}{\partial\eta}C\right)+\frac{\partial}{\partial\eta}\left(\frac{\partial\psi}{\partial\xi}C\right)\right]=\left[\frac{\partial}{\partial\xi}\left(fY\frac{\partial C}{\partial\xi}\right)+\frac{\partial}{\partial\eta}\left(\frac{Y}{f}\frac{\partial C}{\partial\eta}\right)\right]. \tag{14}$$

Here, the liquid flow velocity components necessary for Eq. (13) are calculated from the stream function ψ in the external left-handed (ξ,η) coordinate system by

$$U_\xi=-\frac{1}{YH_\eta}\frac{\partial\psi}{\partial\eta},\quad U_\eta=\frac{1}{YH_\xi}\frac{\partial\psi}{\partial\xi} \tag{15}$$

that was resolved in the first phase of the simulation and is incorporated into Eq. (14). $Pe=2RU/\mathbf{D}$ is the Peclet number and represents the relative magnitude of convection to molecular diffusion. It is known from the numerical simulation of liquid flow in a drop that 4 other non-dimensional parameters, *Re*, *We*, λ and ζ, govern the fluid flow inside and outside the drop with free interface. They exert influence on mass transfer through their effect on flow structure, intensity of convection and shear in the field.

3.2. Initial and boundary conditions

For the situation of mass transfer dominated by the external resistance, the partition coefficient of solute between the drop and the continuous phase is rather large, so that the solute concentration in the drop and at the surface can be reasonably assumed to be zero during the extraction. Considering that the concentration of solute at the remote boundary far away from the drop may be maintained at a constant c^∞, the mass transfer to/from the drop will eventually approach a steady state as the mass transfer proceeds. If only the steady solution is of interest, the partial derivative with respect to time could be dropped from Eq. (14) and the initial condition becomes irrelevant. Thus, the following initial and boundary condition may be assumed for mass transfer from the continuous phase to drops (mass transfer direction $c\to d$):

$$C(\xi,\eta,0)=0\quad\text{at }\theta=0, \tag{16}$$

$$C(1,\eta,\theta)=0\quad\text{at the drop surface, }\xi=1, \tag{17}$$

$$C(0,\eta,\theta)=1\quad\text{at the remote boundary, }\xi=0, \tag{18}$$

$$\frac{\partial C}{\partial\eta}=0\quad\text{on the axis of symmetry, }\eta=0,\ \eta=1. \tag{19}$$

3.3. Mass transfer coefficient

The local diffusive flux N_{loc} is defined and expressed with the local mass transfer coefficient, k_{loc}, as

$$N_{\mathrm{loc}} = -\frac{\mathbf{D}}{h_\xi}\frac{\partial c}{\partial \xi}\bigg|_{\xi=1} = k_{\mathrm{loc}}\left(c^{\infty} - c^{\mathrm{S}}\right). \tag{20}$$

Since the surface concentration c^{S} and the initial concentration in the drop are assumed to be 0, the mass transfer coefficient may be expressed in terms of dimensionless concentration gradient as

$$k_{\mathrm{loc}} = -\frac{\mathbf{D}}{RH_\xi}\frac{\partial C}{\partial \xi}\bigg|_{\xi=1}. \tag{21}$$

Then, the local Sherwood number is

$$Sh_{\mathrm{loc}} = \frac{2Rk_{\mathrm{loc}}}{\mathbf{D}} = -\frac{2}{H_\xi}\frac{\partial C}{\partial \xi}\bigg|_{\xi=1} \tag{22}$$

and the drop surface area average Sh reads

$$Sh = -\frac{2\int_0^1 fY(\partial C/\partial\xi)|_{\xi=1}\,\mathrm{d}\eta}{\int_0^1 YH_\eta\,\mathrm{d}\eta}. \tag{23}$$

3.4. Method for numerical solution

To solve Eq. (14), the control volume formulation described by Patankar [20] was adopted, with the convective term discretized by the power-law scheme.

Multiply Eq. (14) by $\mathrm{d}\xi\,\mathrm{d}\eta\,\mathrm{d}\theta$ and integrate over a control volume $\Delta\xi\Delta\eta$ as depicted in Fig. 3 and the time interval $\Delta\theta$, an algebraic equation for the central node P involved with 4 neighboring nodes N, S, E and W in the form of

$$a_{\mathrm{P}}C_{\mathrm{P}} = a_{\mathrm{E}}C_{\mathrm{E}} + a_{\mathrm{W}}C_{\mathrm{W}} + a_{\mathrm{N}}C_{\mathrm{N}} + a_{\mathrm{S}}C_{\mathrm{S}} + b \tag{24}$$

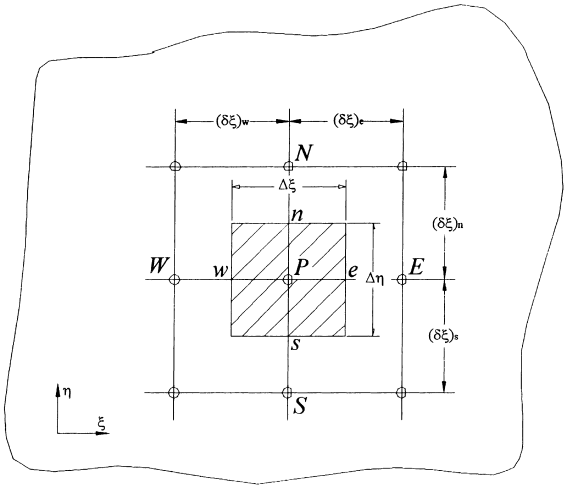

Fig. 3. Stencil of the discretization over a control volume.

is resulted, in which the coefficients are

$$\begin{aligned} a_i &= D_i A(|P_i|) + \|-F_i, 0\|, \quad i = \mathrm{N}, \mathrm{E} \\ a_i &= D_i A(|P_i|) + \|F_i, 0\|, \quad i = \mathrm{S}, \mathrm{W} \end{aligned} \tag{25}$$

and the function $A(x)$ is defined as

$$A(x) = \left\|0.0, (1.0 - 0.1x)^5\right\|, \tag{26}$$

where the operator $\|\cdot\|$ stands for selecting the maximum from all the arguments.

$$b = a_{\mathrm{P}}^0 C^0, \tag{27}$$

$$a_{\mathrm{P}}^0 = \frac{Pe}{2}(H_\xi H_\eta Y)_{\mathrm{P}}\frac{\Delta\xi\Delta\eta}{\Delta\theta}, \tag{28}$$

$$a_{\mathrm{P}} = a_{\mathrm{E}} + a_{\mathrm{W}} + a_{\mathrm{N}} + a_{\mathrm{S}} + a_{\mathrm{P}}^0 \tag{29}$$

with C^0 denoting the concentration of solute at the beginning of the present time step.

According to the power-law scheme, the cell Peclet number is defined as

$$P_i = F_i/D_i, \quad i = \mathrm{n}, \mathrm{s}, \mathrm{e}, \mathrm{w}, \tag{30}$$

$$\begin{aligned} F_i &= \left(-\frac{Pe}{2}\frac{\partial\psi}{\partial\eta}\Delta\eta\right)_i, \quad i = \mathrm{e}, \mathrm{w} \\ F_i &= \left(\frac{Pe}{2}\frac{\partial\psi}{\partial\xi}\Delta\xi\right)_i, \quad i = \mathrm{n}, \mathrm{s} \end{aligned} \tag{31}$$

$$\begin{aligned} D_i &= (fY)_i\frac{\Delta\eta}{\delta\xi_i}, \quad i = \mathrm{e}, \mathrm{w} \\ D_i &= \left(\frac{Y}{f}\right)_i\frac{\Delta\xi}{\delta\eta_i}, \quad i = \mathrm{n}, \mathrm{s}, \end{aligned} \tag{32}$$

where F_{e}, F_{w}, F_{n}, F_{s} are convective fluxes through faces $\mathrm{e}, \mathrm{w}, \mathrm{n}, \mathrm{s}$, and D_{e}, D_{w}, D_{n}, D_{s} are corresponding diffusive fluxes. This differencing scheme is of first-order accuracy in the time domain, and the spatial accuracy is shifted from second order at $P \to 0$ gradually to first order as P increases above 10.

To select the proper spatial mesh density and size of time step to assure the accuracy of numerical simulation of time-dependent mass transfer, Li [8] conducted several numerical tests. Referring also to the results by Mao and Chen [19], an 81×81 spatial grid was sufficiently large and used later in all the numerical solution of fluid flow and mass transfer for a compromise between the numerical accuracy and efficiency. For the simulation of transient mass transfer considered in this work, the dimensionless $\Delta\theta$ below 0.01 was enough to achieve the independence of solution from the time step size. The criterion for the convergence of steady-state solution of mass transfer is the relative change of Sh between successive iterations drops below 1×10^{-6}.

For the limiting case of $Pe \to 0$ of a spherical drop with $Re = 2.2$, $\lambda = 1.0$, $\zeta = 1.1$, numerical simulation gives a result of $Sh = 2.0174$, very close to the analytical solution of $Sh = 2.0$. This may confirm the validity of the present method for simulation.

4. Simulation results and discussion

As compared with the empirical correlation of external mass transfer for liquid drops with intermediate Reynolds number developed for the case of $Re > 70$ and $\lambda < 2$ by Harper and Moore [21],

$$Sh = \frac{2}{\sqrt{\pi}}\left[1 - \frac{1}{Re^{0.5}}\left(2.89 + 2.15\lambda^{0.64}\right)\right]^{0.5} Pe^{0.5}, \qquad (33)$$

good agreement in the range of $0.1 < Pe < 2000$ is evidenced in Fig. 4. When Pe is very large, the transport is dominated by convection, this may lead to very large concentration gradient at the surface. Since the mesh density is limited at the interface, the large gradient of concentration as $\mathbf{D} \to 0$ is not accounted for with sufficient accuracy, and hence, the discrepancy becomes obvious at high Pe region.

Effort is also made to simulate the experimental data by Su et al. [18] and the comparison in the range of $55 \geqslant Re \geqslant 380$, $0.07 \leqslant We \leqslant 1.35$, $1.01 \leqslant \lambda \leqslant 2.07$, $1.20 \leqslant \zeta \leqslant 1.59$, $4.0\times10^4 \leqslant Pe \leqslant 3.9\times10^5$ is rather satisfactory as shown in Fig. 5. Su et al. experimentally measured the mass transfer coefficients for drops of organic phase settling in water in the carbon tetrachloride (*d*rop)–iodine (*s*olute)–water (*c*ontinuous phase) (abbreviated as A-IV), carbon tetrachloride (d)–*o*-nitrophenol (s)–water (c) (A-I) and nitrobenzene (d)–iodine (s)–water (c) (A-III) systems with the purpose to extend the applicability of literature correlations for external drop mass transfer. Since the distribution coefficients

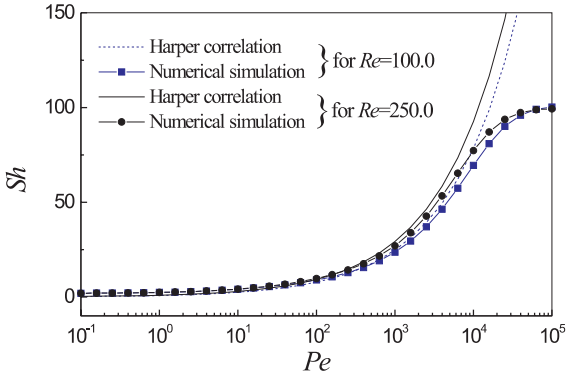

Fig. 4. Comparison of the numerical prediction ($We = 4.0$, $\lambda = 1.1$, $\zeta = 2.0$) and empirical correlation by Harper and Moore [21].

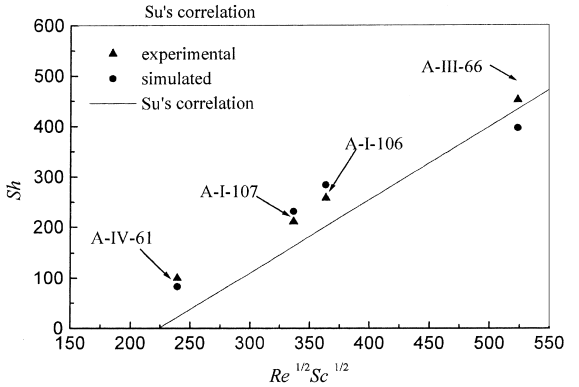

Fig. 5. Comparison of the prediction and Su's correlation $Sh = -325 + 1.45Re^{1/2}Sc^{1/2}$ [18].

are far above 1, the mass transfer can be considered as steady and dominated by mass transfer resistance in the continuous phase. The deviation of simulated results from Su's empirical correlation is considered due to the fact that Su's correlation was based on a large collection of data including oscillating and/or surfactant-contaminated drops. Fig. 6 shows that the simulation is in better agreement with Thorsen's empirical correlation [22] for they paid enough attention to prevent the possible interference of surfactant to the measurements as having been reminded by many previous reports. Unfortunately, large Reynolds number induces unsteady motion of drops (zig-zag motion and shape oscillation), making the current numerical simulation fail for such cases. The current prediction of external mass transfer rate is also in good agreement with the correlation by Garner et al. [23], who carried out experiments on circulating drops in binary systems by the Colburn–Welsh method. The comparison with the Garner correlation has been reported by Li [3], which also supports the present numerical simulation in extraction systems.

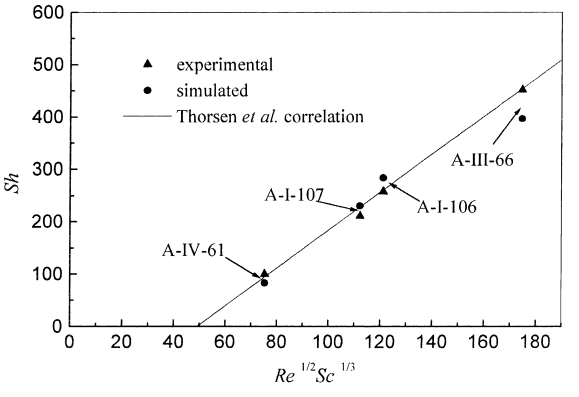

Fig. 6. Comparison of the prediction and Thorsen correlation $Sh = -178 + 3.62Re^{1/2}Sc^{1/3}$ [22].

Figs. 7 and 8 present the flow field and the concentration contour lines for drops with different flow parameters. They indicate that a wake behind the drop appears when the Reynolds number is large enough, but since the Weber number is small, the shape of the drop is still quite spherical. However, a circulating wake promotes the convection of continuous phase in the region around the rear stagnant point and this makes *Sh* increase significantly with the increase of *Re*. The influence of wake on external mass transfer may also be visualized by the distortion of concentration contour lines around the rear stagnancy occurred at higher Reynolds numbers. Garner and Skelland [24] realized that eddy formation at the drop rear may be the main cause of error to correlation of interdrop mass transfer but failed to present convincing evidence. It seems that the numerical simulation of motion and mass transfer for a deformed drop may shed light to the contribution of circulating wake to the external mass transfer as given in the latter part of this section.

Fig. 9 presents the influence of *Re* on the concentration profiles of steady-state mass transfer for drops with $Sc = 10$ and $We = 4$. The upper half is the concentration contour map and the lower part is the streamline drawing. As shown, the concentration contour lines are swept to the downstream direction as *Re* increases. The convection at the drop nose promotes the transport of solute to the drop, making the contour lines compressed spatially, whereas the convection transports solute against the mass transfer by molecular diffusion in the wake, making the contour lines spreading sparsely. As the circulation in the wake develops and becomes strong enough, the concentration contour lines become more and more distorted, and so, a special flow structure is formed.

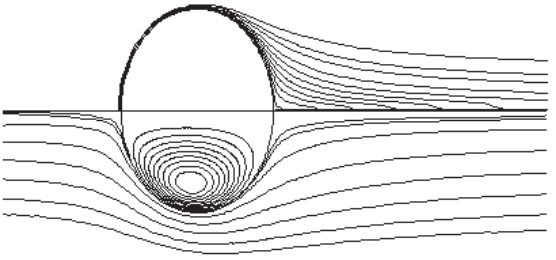

Fig. 7. Concentration and stream function contour of a drop with lower Reynolds number: $Re = 55.5$, $We = 0.07$, $\lambda = 2.07$, $\zeta = 1.20$, $Pe = 3.9 \times 10^4$.

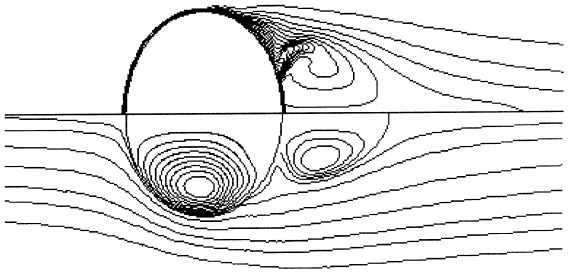

Fig. 8. Concentration and stream function contour of a drop with higher Reynolds number ($Re = 378.4$, $We = 1.32$, $\lambda = 1.01$, $\zeta = 1.59$, $Pe = 2.7 \times 10^5$).

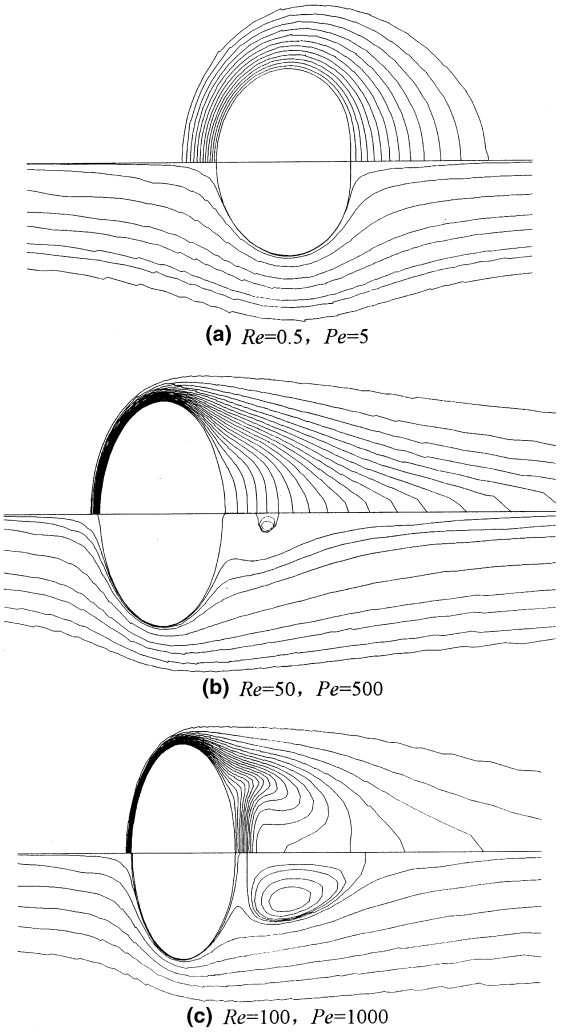

Fig. 9. Influence of *Re* on the flow structure and concentration profile around the drop. The upper part is of concentration profiles and the lower streamlines ($We = 4.0$, $\lambda = 5.0$, $\zeta = 2.0$, $Sc = 10.0$).

It is interesting to note the detail of the flow and concentration fields near the interface for the three cases of drops as described in Fig. 9, the distribution of interfacial shear and the local mass transfer coefficient along the drop surface are plotted against α in

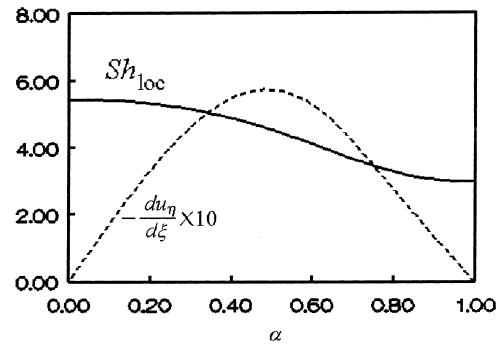

(a) *Re = 0.5*

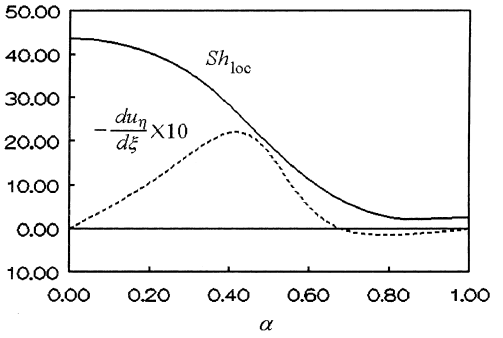

(b) *Re = 50*

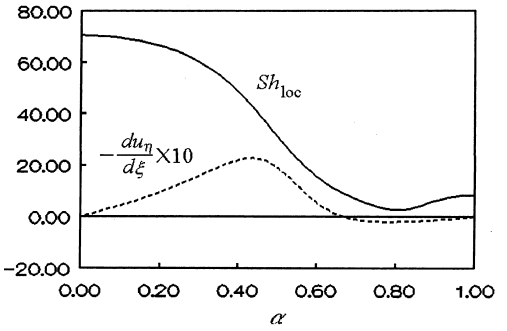

(c) *Re = 100*

Fig. 10. Profiles of interfacial shear and local mass transfer coefficient along the drop surface for drops in Fig. 9.

Fig. 10. α is defined as the angle spanned from the drop nose to a surface location with respect to the drop center and normalized by π. The local Sherwood number at the nose ($\alpha = 0$) is, in general, much higher than that in the rear or wake region (α approaching 1). The convection becomes dominating as *Re* is increased, the difference enlarges gradually, meanwhile the average *Sh* increases too (see Table 1). When a recirculating vortex appears in the wake in Fig. 10(c) with $Re = 100$, the local value of Sh_{loc} first drops down as

Table 1
Mass transfer coefficient and the fraction of active zone of mass transfer for drops depicted in Figs. 9 and 10

Re	*Sh*	$Sh_{loc,min}$	$Sh_{loc,max}$	α_a
0.5	3.583	2.984	5.440	0.574
5.0	6.638	2.241	11.992	0.549
50	18.310	2.153	43.687	0.457
100	30.121	2.550	70.670	0.470

usual, and then increases slightly as the rear stagnant point is approached. This is easily understood in view of the flow structure depicted in Fig. 9, where the strengthened circulation in the wake for case (c) helps the convective diffusion. The sparse distribution of isoconcentration contour lines around the seperation point illustrates the same information of lower value of Sh_{loc}. It is noticed that on the profiles of local Sherwood number the minimum values are very close to 2, which is the lowest value of *Sh* at $Re = 0$ when the external mass transfer is entirely due to molecular diffusion.

The mass transfer is related to the flow structure as documented in Table 1. If the active mass transfer zone is defined by the angle, α_a, spanned from the drop nose to the point defined by

$$Sh_{loc}(0) - Sh_{loc}(\alpha_a) = 0.5(Sh_{max} - Sh_{min}),$$

it is observed that α_a decreases slightly with increasing *Re*. This suggests that the nose region becomes more active and contributive to mass transfer than the rest of interface. When the recirculation in the wake becomes intensive, α_a starts to increase slightly, making only minor contribution to the overall mass transfer rate. The mass transfer contributed by the wake behind the separation point was considered as a separate factor in the correlation of external mass transfer rate. It was represented by the last term in Eq. (34), suggested by Kinard et al. [25], added to the respective terms for radial diffusion (the first term in the right-hand side), natural convection Sh_n (the second term) and the forced convection at the forward part of the drop surface (the third term):

$$Sh = 2.0 + Sh_n + 0.45Re^{0.5}Sc^{1/3} + 0.00484Re\,Sc^{1/3}. \quad (34)$$

From Figs. 10(b) and (c), the pseudo-separation points may be defined by zero interfacial shear rate, and the percentage of the wake mass transfer in the total forced convection is estimated from the numerical simulation to be 95.2% and 95.5%, respectively, for cases (b) and (c). These figures are only in qualitative agreement with the observations cited by Kinard et al. [25].

It is easy to investigate the effect of relevant physical parameters on the average *Sh* by means of numerical

experimentation. Fig. 11 shows that the average *Sh* increases along with *Pe* at different Reynolds numbers. When *Pe* is small, the mass transfer is dominated by molecular diffusion, *Sh* is thence very close to the lower limit of $Sh = 2$. However, *Re* plays a significant role in promoting the rate of mass transfer when *Pe* is large, since the convective transport controls the rate process in this case. It should be kept in mind that when interpreting mass transfer for a given extraction system, *Sc* is predescribed as a constant, where *Re* and *Pe* ($= ReSc$) work in a synchronous way, higher *Re* indicates stronger convection and higher mass transfer rate.

Fig. 12 shows the influence of *Pe* on the concentration profiles under the condition of the same flow structure (i.e., with a fixed value of *Re*). For the case with $Pe \to 0$ as depicted in Fig. 12, the molecular diffusion dominates and the concentration profiles become a set of concentric semicircles, the concentration field is exactly the same result from analytical solution: $Sh = 2.0$. The concentration profiles become unsymmetrical as *Pe* increases. When *Pe* becomes very large, the surface area actively involved with the mass transfer shrinks gradually, and then, the convection plays a more significant role for the mass transport in the wake region. Fig. 13 presents the situation with a circulating wake, and it seems that the larger the value of *Re*, the more severely distorted for the concentration profiles. This suggests that convective mass transfer does play an important role and display certain effect on the surface mass transfer.

Fig. 14 presents the relationship of *Pe* vs. *Sh* under different values of *We*. It is suggested that *We* shows some effect on the external mass transfer as $Pe > 1000$.

The transient mass transfer to a liquid drop is also simulated and the temporal evolution of concentration profiles is presented in Fig. 15. As time goes on, the low

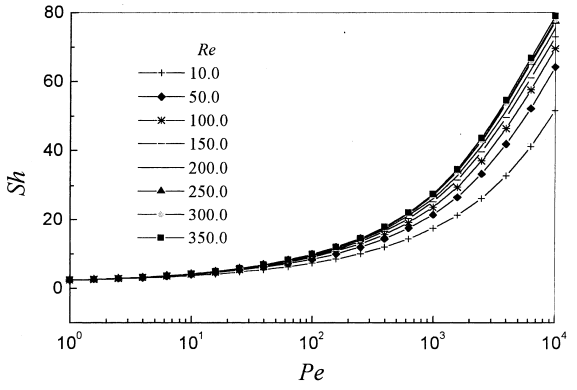

Fig. 11. *Sh* for single drops in laminar flow regime as a function of *Pe* with different Reynolds number ($We = 4.0$, $\lambda = 5.0$, $\zeta = 2.0$).

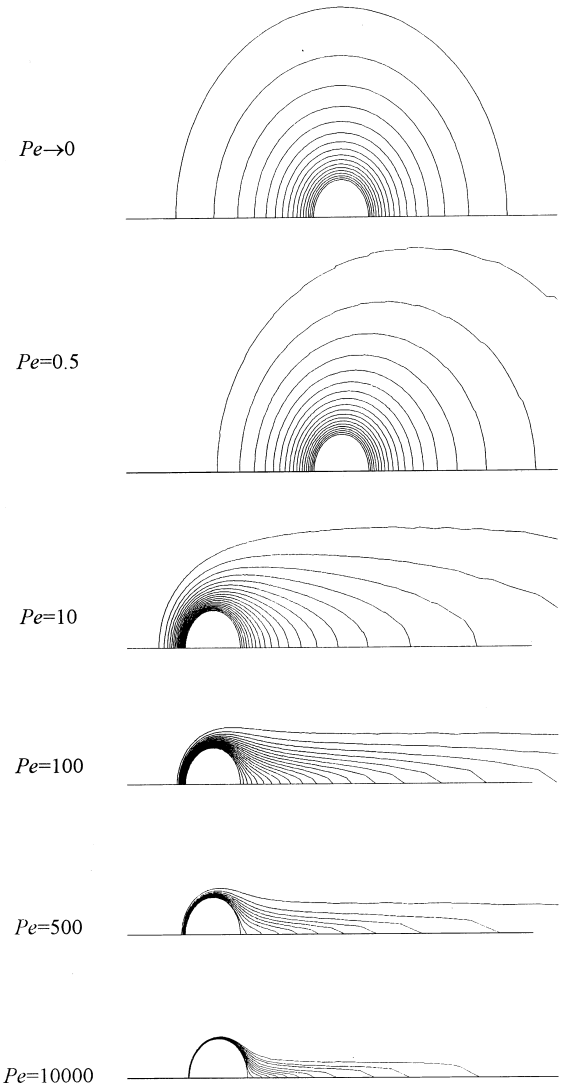

Fig. 12. The influence of *Pe* on the concentration profiles around the liquid drop ($Re = 2.20$, $\lambda = 1.0$, $\zeta = 1.1$).

concentration region (wide spread of concentration contour lines) stretches roughly from the flow separation point, the circulating eddy is actually detached from the drop with mobile interface, and there is no definite separating point on the drop surface in a rigorous sense. As observed from Figs. 8, 9 and 13, all the recirculation zones are detached from drops in coincidence with that of Dandy and Leal [6]. The supply of solute is sufficient to suit the higher local mass transfer coefficient around the drop nose in the upstream region due to strong upstream convection. In the wake, solute supply is limited by rather closed flow recirculation but the depletion of solute is also limited since relatively weak convection and lower local interfacial mass transfer rate. Thus the

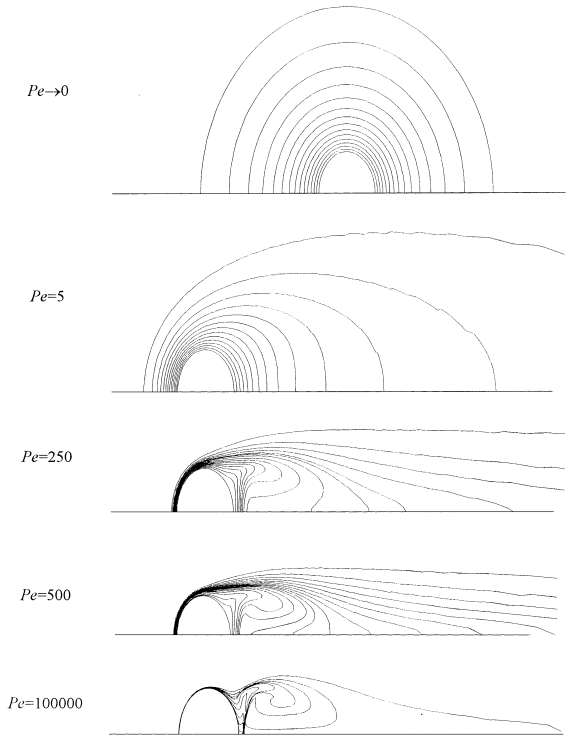

Fig. 13. Influence of Pe on the concentration profiles around a liquid drop with wake ($Re = 150.0$, $We = 2.0$, $\lambda = 5.0$, $\zeta = 2.0$).

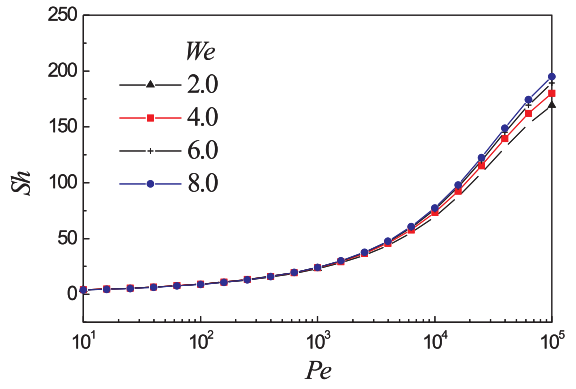

Fig. 14. External Sh for single drop in laminar flow regime as a function of Pe and We ($Re = 150.0$, $\lambda = 5.0$, $\zeta = 2.0$).

rapid local depletion of solute becomes prominent only in the region around the point of flow separation. In the case under investigation, there is a large circulating wake for $Re = 100$ as shown in Fig. 9(c).

For the drops described in Table 1, the temporal decay of instantaneous Sherwood number calculated from simulation is displayed in Fig. 16. Since the cases

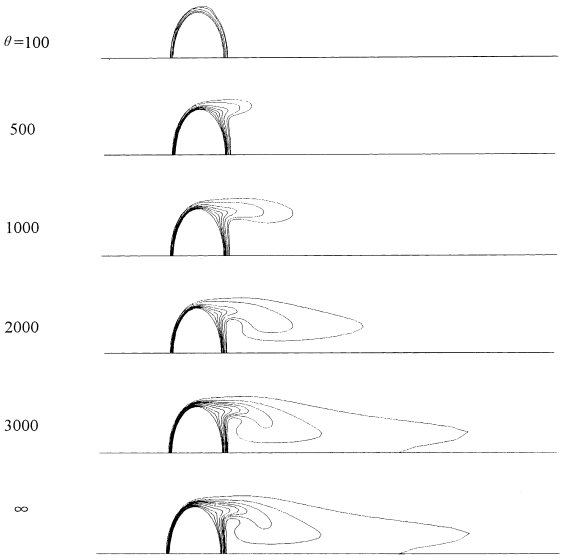

Fig. 15. Influence of mass transfer on the concentration profiles around the drop ($Re = 100.0$, $We = 4.0$, $\lambda = 32.0$, $\zeta = 8.0$, $Pe = 1000$).

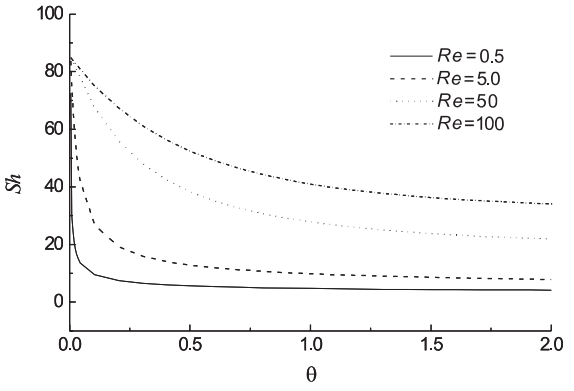

Fig. 16. Typical transient behavior of overall mass transfer coefficient of single drops ($We = 4.0$, $\lambda = 5.0$, $\zeta = 2.0$, $Sc = 10$).

under investigation is with constant Sc, the increase in Re means the progressive dominance by convective mass transfer and suppressed the contribution of molecular diffusive transport. Hence for the case of $Re = 0.5$, it is predominantly controlled by diffusion and the steady-state mass transfer would be reached quickly, while for the case of $Re = 100$, it is convective transport-dominated and Sh approaches very slowly to its steady-state value. It can be noticed from Fig. 16 that the temporal decay of mass transfer coefficient decreases as it approaches the steady-state value. A method is adopted to take the time needed for temporal Sh to decrease by 90% of its total decay in magnitude as the characteristic decay time, $\tau_{0.9}$. Fig. 17 shows the

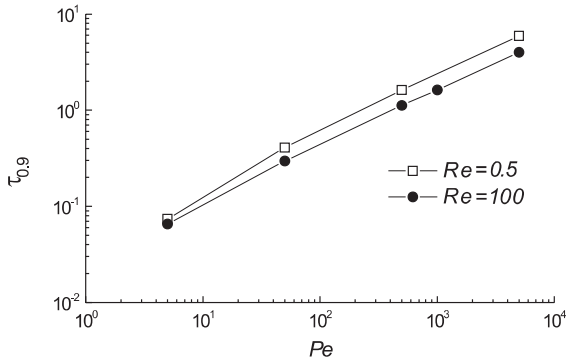

Fig. 17. Characteristic decay time of transient mass transfer versus physical parameters of single drops ($We = 4.0$, $\lambda = 5.0$, $\zeta = 2.0$).

variation of the decay time with *Pe* at two typical values of *Re*. It is observed that the higher **D** (i.e. lower value of *Pe*) demands less time to approach the steady state of external mass transfer, and more intensive convection (higher value of *Re*) is favorable to this transition. The large variation of this characteristic decay time suggests that the drops in extraction equipment should be regenerated at suitable rate so that their life time is close to $\tau_{0.9}$ in order to achieve higher extraction rate at economical expense of agitation power for drop coalescence and redispersion.

5. Conclusions

In a boundary-fitted orthogonal coordinate system, the general governing equations for steady and transient external mass transfer to axisymmetrical single buoyancy-driven drops in steady motion were expanded and numerically solved by the control volume formulation. The numerical simulation for typical cases in low and intermediate range of Reynolds number were presented and compared well with data and empirical correlations in literature. It makes clear that the mathematical formulation of the external mass transfer for a deformable buoyancy-driven drop and the numerical procedures developed in this work can be considered as reasonable. The analysis of the mass transfer coefficient shed light to the respective contribution of molecular diffusion, convection and recirculating wake. The Peclet number will be the major factor controlling the external mass transfer, followed by Reynolds number and Weber number. The simulation of transient external mass transfer and the analysis of the characteristic time scale of decaying instantaneous Sherwood number show that the Peclet number plays a more significant role than the Reynolds number.

Acknowledgements

The financial support from the National Natural Science Foundation of China (Project No. 29792074) and SINOPEC is gratefully acknowledged.

References

[1] R. Clift, J.R. Grace, M.E. Weber, Bubbles, Drops and Particles, Academic Press, San Diego, California, 1978.
[2] A.R. Uribe-Ramirez, W.J. Korchinsky, Single drops: a fundamental approach to the calculation of the velocity profiles and mass transfer rates, in: D.C. Shallcross, R. Paimin, L.M. Prvcic (Eds.), Value Adding Through Solvent Extraction, Proceedings of ISEC'96, The University of Melbourne, Melbourne, 1996, pp. 111–116.
[3] T.W. Li, Numerical simulation of mass transfer of single drops of low or intermediate Reynolds numbers in steady-state motion and its experimental verification, Ph.D. thesis, Institute of Chemical Metallurgy, Chinese Academy of Sciences, Beijing, China, 1998 (in Chinese).
[4] G. Ryskin, L.G. Leal, Numerical solution of free-boundary problems in fluid mechanics Part 2. Buoyancy-driven motion of a gas bubble through a quiescent liquid, Journal of Fluid Mechanics 148 (1984) 19–35.
[5] G. Ryskin, L.G. Leal, Orthogonal mapping, Journal of Computational Physics 50 (1983) 71–100.
[6] D.S. Dandy, L.G. Leal, Buoyancy-driven motion of a deformable drop through a quiescent liquid at intermediate Reynolds numbers, Journal of Fluid Mechanics 208 (1989) 161–192.
[7] T.W. Li, Z.-S. Mao, J.Y. Chen, Simulation of external mass transfer of a single buoyancy-driven drop of intermediate Reynolds numbers, Proceedings of 9th Nat. Conf. Chem. Eng. (NCCE'98), Qingdao, China, 1998, pp. 396–401 (in Chinese).
[8] T.W. Li, C.G. Sun, Z.-S. Mao, J.Y. Chen, Influence of distortion function on the accuracy of numerical simulation of the motion of a single buoyancy-driven deformable drop, Huagong Yejin 20 (1999) 29–37 (in Chinese); Selected Papers of Engineering Chemistry and Metallurgy (China) 1999, Science Press, Beijing, 2000, pp. 92–102 (in English).
[9] M. Miksis, J.M. Vanden-Broeck, J.B. Keller, Axisymmetric bubble or drop in a uniform flow, Journal of Fluid Mechanics 108 (1981) 89–100.
[10] R.J. Haywood, M. Renksizbulut, G.D. Raithby, Transient deformation and evaporation of droplets at intermediate Reynolds numbers, International Journal of Heat and Mass Transfer 37 (1994) 1401–1409.
[11] R.J. Haywood, M. Renksizbulut, G.D. Raithby, G.D. Numerical, solution of deforming evaporating droplets at intermediate Reynolds numbers, Numerical Heat Transfer, Part A 26 (1994) 253–272.
[12] R.M. Wham, O.A. Basaran, C.H. Byers, Wall effects of flow past fluid spheres at finite Reynolds number: wake structure and drag correlations, Chemical Engineering Science 52 (1997) 3345–3367.
[13] A. Tomiyama, I. Zun, A. Sou, T. Sakaguchi, Numerical analysis of bubble motion with the VOF method, Nuclear Engineering and Design 141 (1993) 69–82.

[14] H.K. Zhao, B. Merriman, S. Osher, L.H. Wang, Capturing the behavior of bubbles and drops using the variational level set approach, International Journal of Heat and Mass Transfer 143 (1998) 495–518.
[15] W.Q. Lu, H.C. Chang, An extension of the biharmonic boundary integral method to free surface flow in channels, International Journal of Heat and Mass Transfer 77 (1988) 340–360.
[16] S.W. Welch, Direct simulation of vapor bubble growth, International Journal of Heat and Mass Transfer 41 (1998) 1655–1666.
[17] J.K. Comer, C. Kleinstreuer, Computational analysis of convection heat transfer to non-spherical particles, International Journal of Heat and Mass Transfer 38 (1995) 3171–3180.
[18] Y.F. Su, H.Y. Lu, Z.H. Mao, Study of external mass transfer coefficient of single drops, Huagong Xuebao, (4) (1965) 222–229 (in Chinese).
[19] Z.-S. Mao, J.Y. Chen, Numerical solution of viscous flow past a solid sphere with the control volume formulation, Chinese Journal of Chemical Engineering 5 (1997) 105–116.
[20] S.V. Patankar, Numerical Heat Transfer and Fluid Flow, Wiley and Sons, New York, 1980.
[21] J.F. Harper, D.W. Moore, The motion of a spherical liquid drop at high Reynolds number, Journal of Fluid Mechanics 32 (1968) 367–391.
[22] G. Thorsen, S.G. Terjesen, On the mechanism of mass transfer in liquid–liquid extraction, Chemical Engineering Science 17 (1962) 137–148.
[23] F.H. Garner, A. Foord, M. Tayeban, Mass transfer from circulating liquid drops, Journal of Applied Chemistry 9 (1959) 315–323.
[24] F.H. Garner, A.H.P. Skelland, Mechanism of solute transfer from droplets: liquid–liquid extraction, Industrial and Engineering Chemistry 46 (1954) 1255–1264.
[25] G.E. Kinard, F.S. Manning, W.P. Manning, A new correlation for transfer from single spheres, British Chemical Engineering 8 (1963) 326–327.